Electrical and thermal transport properties of the electron-doped cuprate $Sm_{2-x}Ce_xCuO_{4-y}$ system

D. J. Scanderbeg, B. J. Taylor, R. E. Baumbach, and M. B. Maple
Department of Physics,
University of California, San Diego, La Jolla, CA 92093
(Dated: March 12, 2010)

Electrical and thermal transport measurements were performed on thin films of the electron-doped superconductor $Sm_{2-x}Ce_xCuO_{4-y}$ ($x = 0.13 - 0.19$) in order to study the evolving nature of the charge carriers from the under-doped to over-doped regime. A temperature versus cerium content ($T - x$) phase diagram has been constructed from the electrical transport measurements, yielding a superconducting region similar to that found for other electron-doped superconductors. Thermopower measurements show a dramatic change from the underdoped region ($x < 0.15$) to the overdoped region ($x > 0.15$). Application of the Fisher-Fisher-Huse (FFH) vortex glass scaling model to the magnetoresistance data was found to be insufficient to describe the data in the region of the vortex-solid to vortex-liquid transition. It was found instead that the modified vortex glass scaling model of Rydh, Rapp, and Anderson provided a good description of the data, indicating the importance of the applied field on the pinning landscape. A magnetic field versus temperature ($H - T$) phase diagram has also been constructed for the films with $x \geq 0.14$, displaying the evolution of the vortex glass melting lines $H_g(T)$ across the superconducting regime.

PACS numbers:

I. INTRODUCTION

Establishing a complete $H - T - x$ phase diagram of both hole- and electron-doped high-T_c cuprates is an important step towards building an understanding of the physical origin of superconductivity in these compounds. An immense volume of work has been carried out in this regard for hole-doped cuprates. However, it has been only recently that the electron-doped cuprates have begun to receive similar levels of attention experimentally. Of the class of electron-doped cuprate superconductors having the composition of $R_{2-x}Ce_xCuO_{4\pm\delta}$ (R = La, Pr, Nd, Sm, and Eu), the compounds which received the most attention over the past two decades have been $Nd_{2-x}Ce_xCuO_{4-y}$ and $Pr_{2-x}Ce_xCuO_{4-y}$.[1] The remaining $R_{2-x}Ce_xCuO_{4\pm\delta}$ compounds have seen a recent increase of attention, particularly $Sm_{2-x}Ce_xCuO_{4-y}$, with the mapping of the $T_c - x$ phase diagram,[2] investigation of the pseudogap phase,[3–5] measurements of the superconducting gap energy,[6] and experimental and theoretical investigation of the Fermi surface.[7,8]

This recent work has been primarily concerned with the evolution of the physical properties of $Sm_{2-x}Ce_xCuO_{4-y}$ as a function of Ce content, i.e., the mapping of the $T - x$ phase diagram. There remains, at least, the need to extend investigation of key properties along the 'H-axis,' i.e., to complete the $H - T - x$ phase diagram. Furthermore, the Sm^{3+} ions in $Sm_{2-x}Ce_xCuO_{4-y}$ order antiferromagnetically below the Néel temperature $T_N \sim 6$ K into an arrangement that is unique in high-T_c materials, wherein the magnetic moment of the Sm^{3+} sites align within a single ab plane ferromagnetically, but each adjacent plane along the c-axis is aligned antiferromagnetically.[9] This presents an opportunity to both investigate the interplay of superconductivity and magnetism and the possible role of magnetic excitations in the pairing process,[10,11] and, also to study of the effect of magnetic order on the dynamic properties vortices in the region of the melting of the vortex solid.

We report here electrical and thermal transport measurements on thin films of $Sm_{2-x}Ce_xCuO_{4-y}$ ($x = 0.13 - 0.19$) in order to study the progression of key physical properties from the under-doped to over-doped regime. We find similar features in the evolution of thermopower properties as that found for films of $Pr_{2-x}Ce_xCuO_{4-y}$,[12] which has been taken as evidence for the presence of both holes and electrons as charge carriers. From high field ab-plane resistivity $\rho(T)$ measurements we determine the pseudogap temperature T^* across the under-doped to over-doped regimes. Finally, from an analysis of the vortex glass melting transition we find that the pinning landscape in the $H - T$ plane of $Sm_{2-x}Ce_xCuO_{4-y}$ is significantly affected by the application of the magnetic field, a possible indication of the interaction of Sm^{3+} moments with the magnetic flux line lattice.

II. EXPERIMENTAL DETAILS

Polycrystalline $Sm_{2-x}Ce_xCuO_{4-y}$ target material for use in the pulsed laser deposition (PLD) process was formed by a solid state reaction technique with starting materials of 99.99% pure oxides of Sm_2O_3, the dopant CeO_2, and CuO. To insure the proper stoichiometry of the target the powders were dried in air inside alumina crucibles at 900 °C for $\geq$ 12 hours since both compunds are known to absorb water readily.[13] Once dry, the starting materials were weighed and mixed in ultra-high purity (UHP) Ar atmosphere. The prepared mixture was

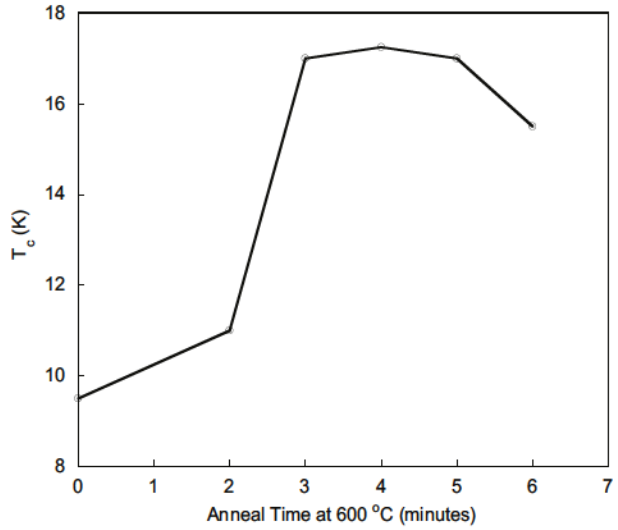

FIG. 1: Superconducting critical temperature T_c versus anneal (dwell) time at 600 °C for the $x = 0.16$ samples. An optimal anneal time of 4 minutes was also found for all other concentrations grown.

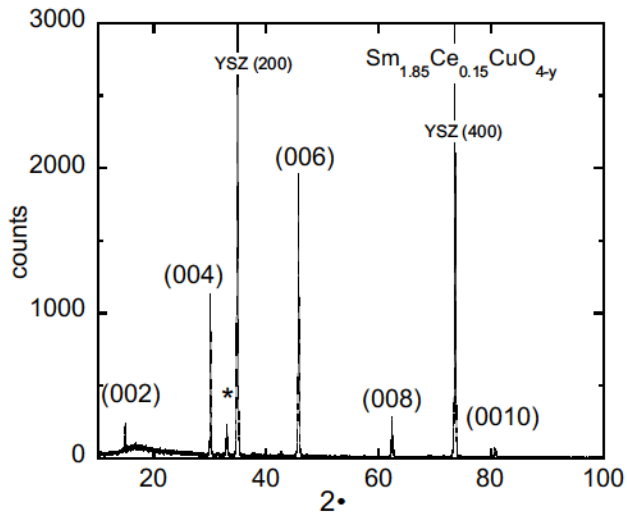

FIG. 2: X-ray diffraction pattern for a $Sm_{1.85}Ce_{0.15}CuO_{4-y}$ film exhibiting the highly c-axis oriented nature of the films. An impurity peak (indicated with an asterisk) seen at $\sim 33°$ is identified as CeO_2. Other very small peaks observed are identified as being attributable to the impurity presence of either CeO_2 or Ce_2O_3. Two substrate peaks are visible at $\sim 35°$ and $\sim 73°$. X-ray diffraction data for all concentrations grown indicated a similarly high quality of the films.

fired in air for $\geq$ 18 hours at 900 °C in an alumina crucible, then ground by hand and re-fired in air at 1000 °C for $\geq$ 24 hours. Subsequently, the material was ground in a centrifugal ball mill, and the resulting fine powder was pressed into a pellet and fired a final time in air at 1100 °C for $\geq$ 3 days. Finally, the furnace was cooled to 900 °C and the target was removed to cool in air.

The $Sm_{2-x}Ce_xCuO_{4-y}$ films were grown on yttria-stabilized zirconia (YSZ) with a (100) orientation. The optimal growth conditions of the films for each concentration of $Sm_{2-x}Ce_xCuO_{4-y}$ were determined experimentally from numerous trial growths while systematically varying the parameters including: incident laser energy density, substrate temperature, chamber pressure, and annealing conditions. The optimal incident laser energy density was determined to be ~ 1.5 J/cm^2. The energy density was verified before and after each growth using a Scientech Vector S310 external power meter. All concentrations of the films form well at T $\approx$ 800 °C and under chamber pressures of $p \approx 200$ mTorr of flowing N_2O. The N_2O gas was flowed directly into the plume of the laser ablated material. The deposition time was 10 minutes in duration for all samples. After each deposition the chamber was immediately evacuated to $p < 10^{-6}$ torr and the samples were also immediately cooled to 600 °C at a rate of 20 °C/min. The samples dwelled at 600 °C for a duration of zero to 10 minutes, cooled again to 400 °C at a rate of 25 °C/min, dwelled for 8 minutes, and then the heater was shut off and the samples cooled to $\sim$ 100 °C before venting the chamber and removing the films. A plot of the superconducting critical temperature, T_c, versus anneal time is shown in Fig. (1) for the $x = 0.16$ sample. T_c is shown to increase with dwell time to a maximum at about 4 minutes. An optimal anneal time of $\approx$ 4 minutes at 600 °C was found for all other concentrations as well. We note here that a finite 'shelf life' seems to be at work for all $Sm_{2-x}Ce_xCuO_{4-y}$ films grown here (and in other studies we have undertaken). Samples left exposed to the atmosphere experience a sudden rapid deterioration throughout the entire film after approximately 9 - 12 months – upon which the superconducting properties are irretrievably lost – leaving behind a transparent film. The shelf life of samples stored in a UHP argon atmosphere is extended to about 18 months, however the breakdown appears to be inevitable. All data presented here were taken from samples that were from 1 week to 3 months old, and were stored in a $\sim$1 torr vacuum in the intervening time between sample growth and measurement.

All films were characterized by x-ray diffraction and electrical transport measurements. Magnetization $M(T)$ measurements (not shown) were also performed as part of the growth optimization process to establish T_c values. All resistivity $\rho(H,T)$ data were taken on films in which gold pads were sputtered on the as grown films in a standard 4-wire configuration. The films were annealed for 10 minutes in air at 500 °C to allow the gold to diffuse into the films. Gold leads were attached using a two part silver epoxy and cured for 3 minutes at 200 °C. Typical sample dimensions are $\ell \times w \times t \approx 3\,\text{mm} \times 3\,\text{mm} \times 100\,\text{nm}$. Thermopower measurements were also performed on as grown samples on a modified Quantum Design PPMS electrical transport puck, as described further below. Electrical transport measurements were performed with a Keithley 220

programmable current source and a Keithley 2182 nanovoltmeter with the samples in a Quantum Design PPMS over a temperature range 1.85 K $\leq T \leq$ 310 K and magnetic field H range up to 9T.

Standard $\theta - 2\theta$ measurements were made using a Rigaku DMAXB x-ray diffractometer. X-ray data for the $x = 0.15$ sample is shown in Fig. (2). The diffraction patterns are consistent for all samples and, in addition to the substrate peaks, the major peaks are associated with the (001) reflections, indicating excellent c-axis orientation. There are two primary minor peaks consistently observed which we associate with an impurity phase. These peaks were minimized during growth optimization; however, they could never be completely removed. All of the minor peaks observed can be attributed to the presence of CeO_2 or Ce_2O_3. In a recent study by Kang et al.,[14] it is suggested that, rather than being a materials processing problem, the rare earth oxide "impurity phase" is actually responsible for superconductivity in the electron-doped compounds. The authors propose that, during the high temperature oxygen reducing anneal process the compound phase separates into this small Cu free "impurity phase" and a "Cu-perfect" $Ln_{2-x}Ce_xCuO_{4-y}$ phase. Effectively, this allows any Cu vacancies in the $Ln_{2-x}Ce_xCuO_{4-y}$ phase to be filled by the Cu atoms freed in the phase separation and creation of the Cu free R_2O_3 phase.

III. EXPERIMENTAL RESULTS

A. Thermopower

Similar to the Hall effect, the thermopower of a material is related to the carrier concentration and charge carrier type in a material with $S \propto 1/ne$, where n is the carrier concentration and e is the charge of the carrier. Thermopower measurements of high T_c cuprate materials can potentially shed light on the nature of the charge carriers in both hole-doped and electron-doped compounds and on how they evolve across the doping spectrum.

Thermopower data are shown in Fig. (3) for samples with cerium concentrations of $x = 0.135$, 0.14, 0.15, 0.16, and 0.19. It can be seen that there is a dramatic change in the thermopower as we move from the underdoped to the overdoped concentrations. The underdoped samples exhibit a negative thermopower whose magnitude decreases as the optimal T_c doping level ($x = 0.15$) is approached. Additionally, it is seen that the thermopower for the $x = 0.15$ sample is very small in magnitude and negative at low temperatures and has a sign change at $T \approx 35$ K. We compare the data here to thermopower measurements on polycrystalline $Sm_{2-x}Ce_xCuO_{4-y}$ and thin films of $Pr_{2-x}Ce_xCuO_{4-y}$.

Yang et al.[15] performed some of the earliest thermopower measurements of polycrystalline $Sm_{2-x}Ce_xCuO_{4-y}$ samples across a wide doping spectrum. In the underdoped limit, the samples were found

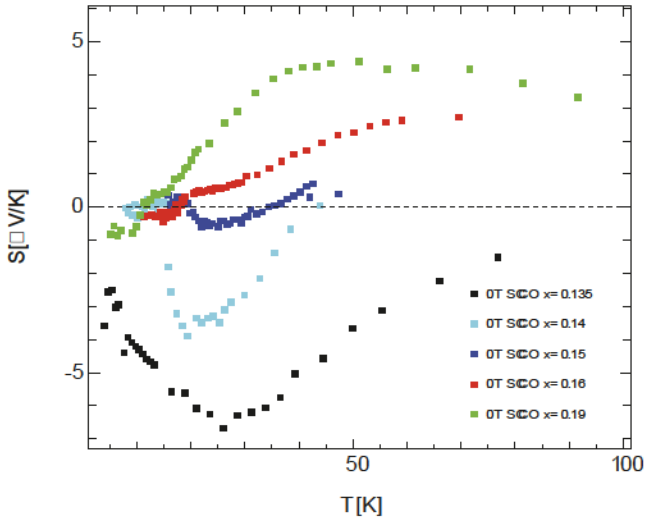

FIG. 3: Thermopower data of $Sm_{2-x}Ce_xCuO_{4-y}$ films with Ce content $x = 0.135$, 0.14, 0.15, 0.16, and 0.19.

to have a large negative thermopower voltage, implying n-type carriers. The magnitude of the thermopower voltage decreased as the Ce content was increased until optimal doping at $x = 0.15$ where there was a sign change and a small positive signal (on the order of 1 μV/K) was observed. This small positive signal peaked and then remained at $S \approx 0.5$ μV/K up to room temperature. Moving beyond optimal doping ($x > 0.15$), the thermopower voltage retained the same shape as that of the $x = 0.15$ sample; however, there was a sign change at higher temperature with a small magnitude (S ≤ 1 μV/K) negative voltage.

Recent thermopower measurements performed by Li et al.[12] on thin films of $Pr_{2-x}Ce_xCuO_{4-y}$ were observed to be consistent with Hall effect measurements performed on the same samples.[16] It was shown that the sign change in the thermopower was at the same temperature as that of Hall effect measurements, from which the presence of both holes and electrons as charge carriers can be inferred. The thermopower was observed to have a large negative value for underdoped films, decreasing in magnitude until the $x = 0.16$ overdoped sample, where the thermopower is positive above T_c until $T \approx 25$ K where it changes sign. Samples with $x > 0.16$ show a small positive value of S for all temperatures above T_c. These results were taken as evidence for an antiferromagnetic to paramagnetic quantum phase transition in electron-doped cuprates near x = 0.16.

The results found here bear some similarities to the results from the thermopower study of polycrystalline $Sm_{2-x}Ce_xCuO_{4-y}$ samples, however, a more consistent comparison can be made to results from $Pr_{2-x}Ce_xCuO_{4-y}$ thin films. One possible reason for the difference is in the nature of the samples themselves, since both thin film studies produced c-axis oriented films and measurements were performed in the ab-plane. The differences with the polycrystalline $Sm_{2-x}Ce_xCuO_{4-y}$

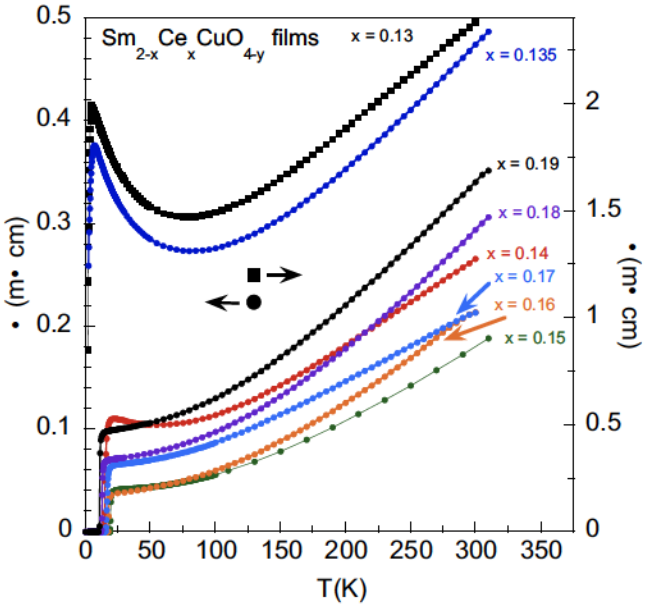

FIG. 4: (color online) Resistivity $\rho(T)$ in zero magnetic field for thin film samples of $Sm_{2-x}Ce_xCuO_{4-y}$ with x = 0.13 - 0.19.

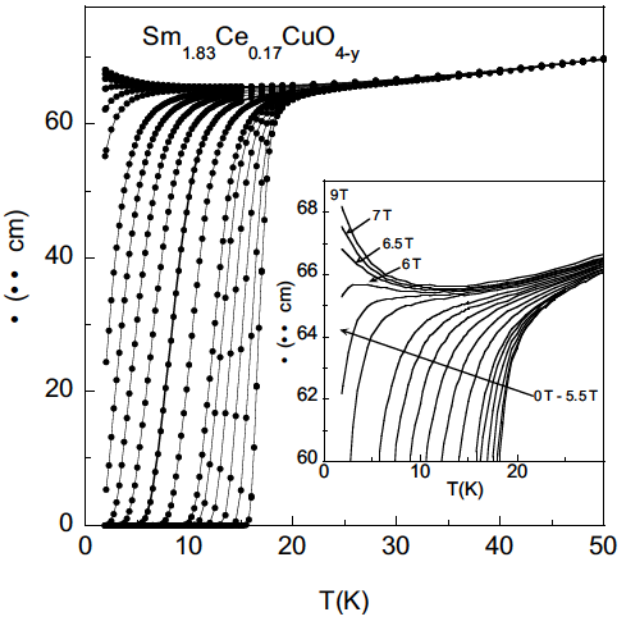

FIG. 5: Resistivity $\rho(T)$ in magnetic fields up to 9 T for the $x = 0.17$ sample. The data shown are taken in magnetic fields of 0 T to 0.8 T in 0.2 T increments, 1.0 T to 7 T in 0.5 T increments, and at 9 T. Additional $\rho(H)$ vs. T data were taken at other fields not shown here.

study can likely be attributed to the different orientations of the grains and, possible oxygen inhomogeneities within the grains. However, further comparison of our data with that of the $Pr_{2-x}Ce_xCuO_{4-y}$ thin films show that the only significant difference is the cerium concentration at which there is a sign change in the thermopower. This is observed at optimal doping $x = 0.15$ for $Sm_{2-x}Ce_xCuO_{4-y}$ as opposed to $x = 0.16$ for $Pr_{2-x}Ce_xCuO_{4-y}$. Qualitatively, the data behave as one would expect up to about optimal doping, wherein an increase of the cerium content in the samples should result in a proportional increase in the (electron) carrier concentration. With the thermopower inversely proportional to the carrier concentration, the magnitude of the thermopower is then normally expected to decrease with increased Ce doping. In all of the samples mentioned above, there is a sign change in the measured thermopower voltage as a function of cerium concentration. In both cases, this was explained in terms of a two-band model with a compensation at some critical doping level (x_c), above which the hole contribution dominates. As the data presented here on $Sm_{2-x}Ce_xCuO_{4-y}$ film samples appear to be most consistent with the corresponding data from $Pr_{2-x}Ce_xCuO_{4-y}$ films this would lead us to also invoke a two-band model. This conclusion should be taken in the context of recent quantum oscillation experiments on the electron doped superconductor $Nd_{2-x}Ce_xCuO_{4-y}$[17] and on hole-doped high-T_c cuprates, which have been interpreted as evidence for two conduction bands at the Fermi surface consisting of both holes[18] and electrons[19,20]. The possible existence of two-band superconductivity in both hole- and electron-doped cuprates suggests an important electronic commonality in spite of other known differences in their electronic structures and superconducting phase diagrams.

B. Electrical Transport Measurements

1. $H - T_c - x$ phase diagram

Measurements of resistivity ρ vs. temperature in zero magnetic field of all samples are shown in Fig. (4). The superconducting transition temperature T_c for each of the films, shown in Fig. (8), was taken as the temperature at which the resistivity drops to 50% of the normal state value at temperatures just above the transition. The transition width, ΔT_c, is taken as the difference in temperature between the 10% - 90% drop in the normal state resistivity values. The values of the critical temperatures determined by the mid point transition $T_c(\mathrm{K})_{[\mathrm{mid}]}$ for all samples are given in Table I.

Resistivity $\rho(T)$ measurements in fixed magnetic fields up to 9 T were performed on each $Sm_{2-x}Ce_xCuO_{4-y}$ film. In Fig. (5) we show $\rho(T)$ data for the $x = 0.17$ sample. As more easily seen in the inset, as superconductivity is suppressed by increasing the magnetic field, the resistivity begins to exhibit a clear upturn at low temperatures. This upturn is observed in the high field $\rho(T)$ data of each sample. As shown in Fig. (4), the zero field resistivity data of the underdoped samples already exhibit such an upturn, prior to the transition into the superconducting state. Interestingly though, we find that the high field data ($H \gtrsim 7\,\mathrm{T}$) for all samples, under-

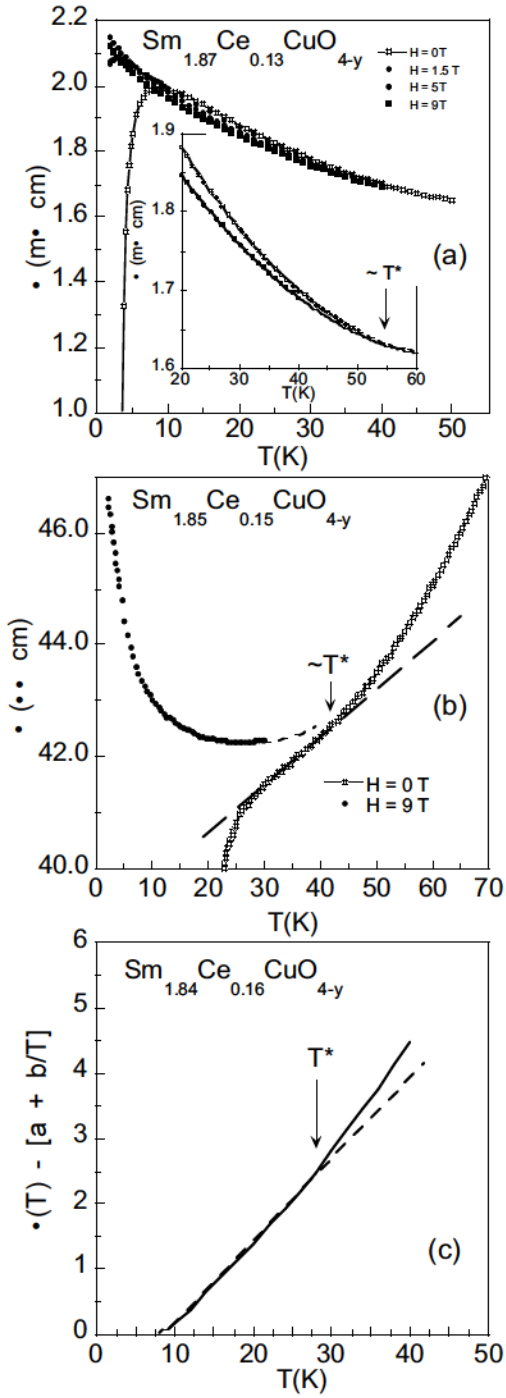

FIG. 6: In field ($H = 9$ T) resistivity data from which the pseudogap temperature T^* is inferred for $Sm_{2-x}Ce_xCuO_{4-y}$ thin film samples $x = 0.13, 0.15$ and 0.16. See the text for further explanation of the criteria by which T^* was established.

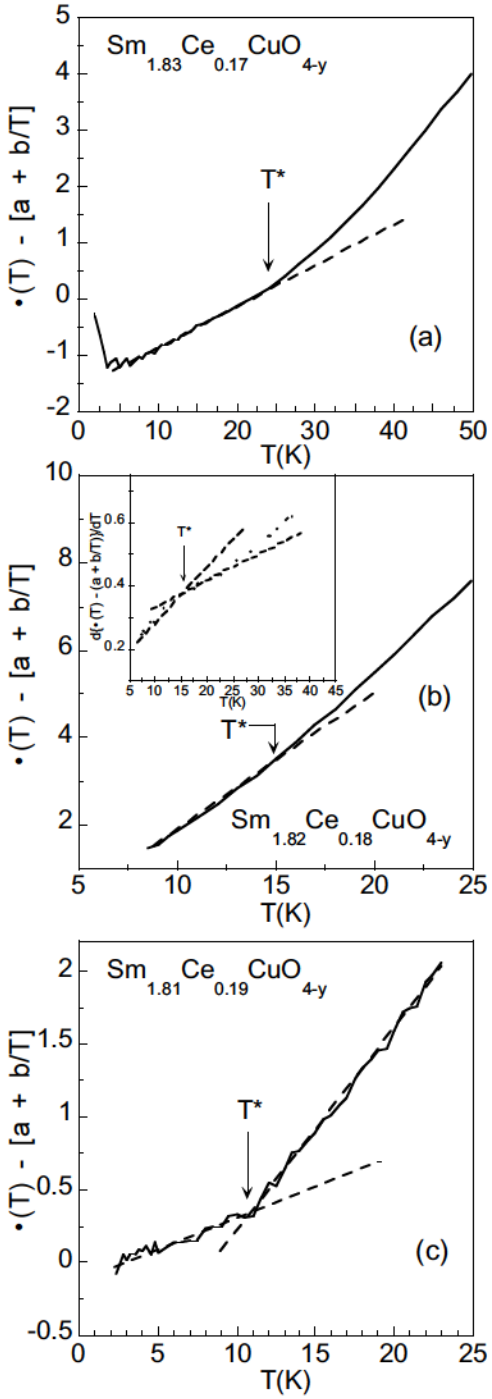

FIG. 7: In field ($H = 9$ T) resistivity data from which the pseudogap temperature T^* is inferred for $Sm_{2-x}Ce_xCuO_{4-y}$ thin film samples $x = 0.17, 0.18$ and 0.19. See the text for further explanation of the criteria by which T^* was established.

doped to overdoped, can be fit well to an empirical expression $\rho(T) = \rho_0 + a/T + bT + cT^2$ from $T = 2$ K (the lowest temperaturs measured) up to temperatures well above (40 K $\lesssim T \lesssim 160$ K) the critical temperature T_c.

The low temperature-high field behavior observed here across the doping range $x = 0.13$ - 0.19 of $Sm_{2-x}Ce_xCuO_{4-y}$ is in marked contrast to that found for the electron doped cuprate systems $La_{2-x}Ce_xCuO_4$ and $Pr_{2-x}Ce_xCuO_{4-y}$, where an insulator-to-metal transition is observed to occur near optimal doping via resistivity measurements in large magnetic fields.[21–23] At a concentration of $x = 0.17$ the high field resistivity $\rho(T)$

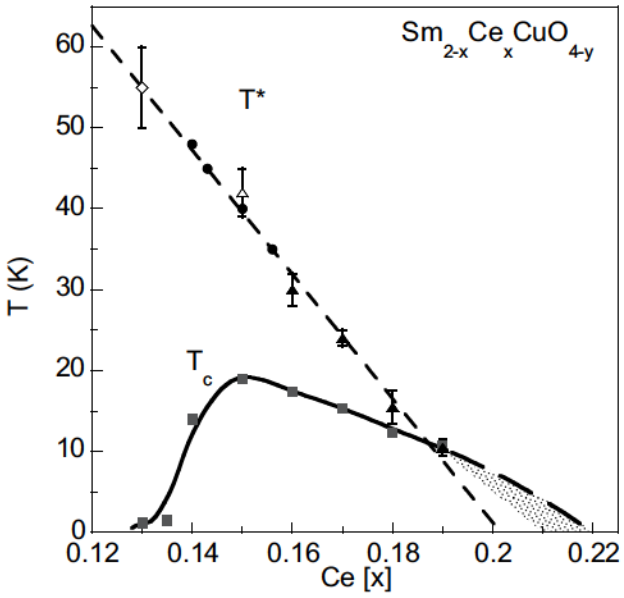

FIG. 8: Superconducting transition temperature T_c (squares) versus cerium concentration, x, for $Sm_{2-x}Ce_xCuO_{4-y}$ thin film samples with $x = 0.13$ to $x = 0.19$. The solid line is a guide to the eye. Also shown is the pseudogap temperature T^* vs x as determined from analysis of the resistivity data of the $Sm_{2-x}Ce_xCuO_{4-y}$ films (closed triangles, open triangle, open diamond) as indicated in Figs. (6) and (7), and as determined by Kawakami et al.,[4] from c-axis electrical transport measurements performed on $Sm_{2-x}Ce_xCuO_{4-y}$ single crystals (circles). The dashed line is a linear fit to the T^* data. The shaded section indicates the region over which there is a possible difference between the T_c vs x result found here and that found for MBE-grown films,[2] as described in the text.

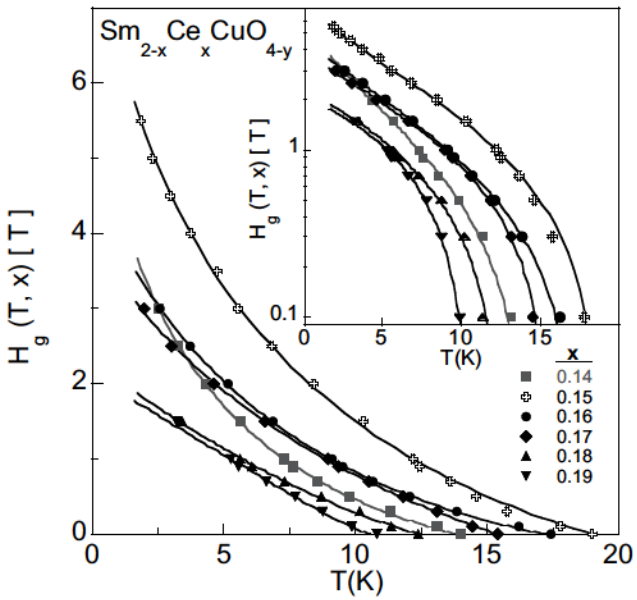

FIG. 9: Vortex glass melting lines, $H_g(T)$, determined via analysis in the context of the RRA model, for each cerium concentration x, with x = 0.14 to x = 0.19. Inset: Same data as in the main panel, plotted on a semi-log scale. The solid curves shown are fits to the data by the empirical expression for the vortex glass melting line found by Taylor and Maple in ref. [25], as recently reported by Taylor et. al., in ref. [26]. Values of the fitting parameters can also be found in ref. [26].

of $La_{2-x}Ce_xCuO_4$ and $Pr_{2-x}Ce_xCuO_{4-y}$ monotonically decreases to a residual value with a $\rho(T) \sim T^n$ dependence with $n > 1$ and $n = 1$ respectively. It would appear that the persistence of an insulating-like component in the resistivity $\rho(T)$ in samples with Ce concentrations up to at least $x = 0.19$ is unique to the $Sm_{2-x}Ce_xCuO_{4-y}$ system. We note that for both the $La_{2-x}Ce_xCuO_4$ and $Pr_{2-x}Ce_xCuO_{4-y}$ system, the characteristic temperature $T_{min}(x)$, corresponding to an observed local minimum in the $\rho_{ab}(T)$ $(H = 0)$ data, vanishes in the vicinity of $x = 0.15$.[22,24] The temperature $T_{min}(x)$ is frequently taken as being indicative of the presence of the pseudogap, where $T_{min}(x) \lesssim T^*(x)$.

In Figs. (6) and (7) we show analysis of the resistivity data of the $Sm_{2-x}Ce_xCuO_{4-y}$ films from which we infer the location of the pseudogap temperature T^* for each film, excluding the $x = 0.135$ and 0.14 samples. For the $x = 0.16 - 0.19$ samples, $T^*(x)$ is determined by the temperature at which a distinct 'kink' is observed when the constant ρ_0 and T^{-1} terms are subtracted from the high field $(H = 9T)$ resistivity vs temperature data, i.e., $\rho(T) - (\rho_0 + a/T)$. This feature is clearly visible for the $x = 0.17$ and $x = 0.19$ samples. For the $x = 0.18$ sample we have also plotted (Fig (7b) inset) $d\{\rho(T) - (\rho_0 + a/T)\}/dT$ vs T wherein the 'kink' is more pronounced.

As noted above, all of the $Sm_{2-x}Ce_xCuO_{4-y}$ films that we have grown are subject to a shelf life that limits the time period over which measurements can be performed. Unfortunately, the high field data of the $x = 0.13 - 0.15$ samples does not extend to temperatures high enough by which we can perform the same analysis as done for the $x = 0.16 - 0.19$ films. These films have since exceed their shelf life, thus further measurements can not be performed. However, we find that we can extract meaningful values for T^* for the $x = 0.13$ and $x = 0.15$ through the following procedure: For the $x = 0.13$ sample we observe at low temperatures (still above T_c) a negative magnetoresistive response that decreases in magnitude as temperature is increased. This behavior is similar to the $\rho_c(T)$ data taken in various magnetic fields by Kawakami on single crystals of $Sm_{2-x}Ce_xCuO_{4-y}$ from which the pseudogap temperature for this system was inferred in the doping range $0.14 \leq x \leq 0.156$ by the temperature at which a negative magnetoresistance was observed, increasing in magnitude to lower temperatures.[3] It seems likely that, due to some roughness of the sample surface, the measured resistivity of this film contains a small ρ_c component, to which we attribute the observed negative magnetoresistance. The in field resistivity $\rho(T)$ data taken here does not extend to a temperature high enough to directly determine T^* by the point at which the zero

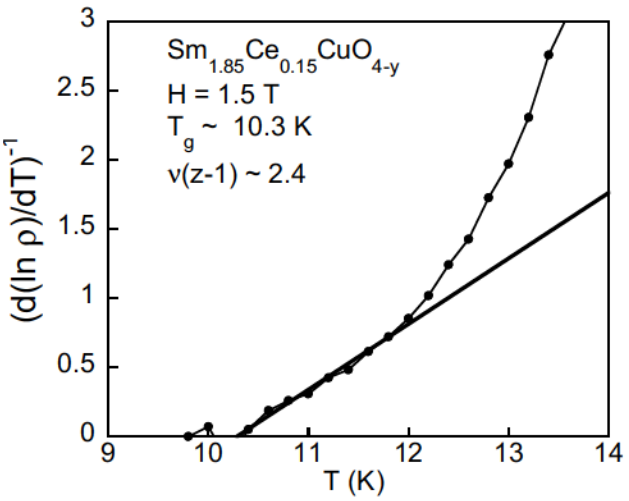

FIG. 10: Scaled resistivity dln ρ/dT vs T for the optimally doped $Sm_{1.85}Ce_{0.15}CuO_{4-y}$ sample. The dark line is a guide to the eye through the region to which a linear fit was applied.

field and high field data merge, however we obtain a reasonable estimate by an extrapolation of the data as shown in the inset of Fig. (6a). For the $x = 0.15$ sample, we have determined an estimate for T^* by extrapolating the 9 T $\rho(T)$ data to higher temperatures, and by the location of an inflection point observed in the $(H = 0)$ $\rho(T)$ data (Fig (6b)). The values for $T^*(x)$ determined here are given in Table I, and shown in Fig (8) along with the data of Kawakami et al.[4]

From the above zero field and high field $\rho(T)$ data, we construct in Fig. (8) a temperature T versus Ce concentration x phase diagram. Our results for T_c are found to be comparable to a recent $T_c - x$ phase diagram constructed by Krockenberger et al.,[2] for MBE-grown expitaxial thin films of $Sm_{2-x}Ce_xCuO_{4-y}$. There is good agreement between the transition temperatures T_c of samples in the $x = 0.15 - 0.17$ range produced from both growth methods. There is also good agreement as to the Ce concetration in the underdoped region at which superconductivity emerges: in the range of $x \approx 0.125$ (here) to $x \approx 0.13$ (MBE-films). However, there appears to be a disagreement as to the temperature in the overdoped region at which the superconducting dome terminates. We obtain higher values of T_c for $x \geq 0.18$, resulting in an *extrapolated* critical upper concentration of $x \approx 0.22$ that is somewhat higher than that of the experimentally determined value of $x \approx 0.21$ for the MBE-films. In either case, this places the linearly extrapolated $T^* = 0$ K pseudogap temperature, at $x \approx 0.20$, i.e., within the superconducting 'dome.' This result is relevant in the context of the many competing scenarios as to the relationship of the pseudogap phase to the superconducting state.[27,28]

2. *Vortex-glass Scaling Analysis*

From the above in field $\rho(T)$ measurements the vortex-solid to vortex-liquid transition boundary, $H_g(T)$, shown in Fig. (9), was determined for samples with $0.14 \leq x \leq 0.19$. The shape of this boundary in the underdoped region has an upward curvature with decreasing temperature that is typically reported for high-T_c compounds.[29] However, as the system progresses into the overdoped region, the $H_g(T)$ line rapidly loses this steep upward curvature, developing a form approaching that of the upper critical field $H_{c2}(T)$ a conventional BCS two-band superconductor.[30]

The magnetoresistance data were further analyzed in the context of the Fisher-Fisher-Huse (FFH) vortex glass scaling model.[31] In the critical region, at temperatures above the vortex glass melting temperature T_g, the resistivity conforms to an equation of the form: $\rho = \rho_0 |T/T_g - 1|^{\nu(z+2-d)}$. Assuming $d = 3$ gives: $\rho = \rho_0 |T/T_g - 1|^{\nu(z-1)}$. When performing an analysis of in field resistivity data in the context of the FFH model, a plot of (dln ρ/dT)$^{-1}$ vs T, is used to clearly identify a region of linear behavior – corresponding to the critical region of the vortex glass melting transition – from which the values of T_g and $\nu(z-1)$ can be extracted. This scaling analysis was performed on the data for each magnetic field applied to the samples with cerium concentration $x \geq 0.14$. A plot of (dln ρ/dT)$^{-1}$ vs T for the $Sm_{1.85}Ce_{0.15}CuO_{4-y}$ sample is shown in Fig. (10). It can be seen that a region of *linearly* vanishing data is not readily apparent. This result is typical of all the $H_g(T)$ data analyzed in this manner, suggesting that the vortex glass melting transition scenario may not be adequate for describing the vortex-solid to vortex-liquid transition of the $Sm_{2-x}Ce_xCuO_{4-y}$ system. In addition to the Fisher-Fisher-Huse (FFH) model, a modified vortex glass theory proposed by Rydh, Rapp, and Andersson (RRA)[32,33] was also used to analyze the data. From the RRA model, (which is based upon the FFH model), a modified scaling expression for the resistivity in the critical region is obtained such that,

$$\rho(T) = \rho_0 \left| \frac{T(T_c - T_g)}{T_g(T_c - T)} - 1 \right|^{\nu(z-1)}, \qquad (1)$$

where ρ_0 is taken as the normal state resistivity just above T_c. The RRA model differs from the FFH model in that the authors claim that the pinning energy scale changes with both temperature and magnetic field such that the vortex glass transition is dependent on the energy difference $k_BT - U_0(H,T)$, where U_0 is the current independent mean pinning energy. Qualitatively speaking, this can be thought of in terms of using the two dimensional distance in the $H - T$ plane to traverse to T_g, instead of taking the usual one dimensional distance in temperature to T_g at a constant field H. By plotting ρ/ρ_n vs $[T(T_c\text{-}T_g)/T_g(T_c\text{-}T)$ - 1] on a log-log plot,

TABLE I: Values of the superconducting critical temperature at the midpoint of the transition and at the vanishing of the resistivity, $T_c(\mathrm{K})_{[\mathrm{mid}]}$ and $T_c(\mathrm{K})_{[\rho\to 0]}$, respectively, the superconducting transition width, ΔT_c, the pseudogap temperature T^*, the critical exponent $s \equiv \nu(z-1)$, and the estimated error of s, Δs, for each Ce concentration x.

x	$T_c(\mathrm{K})_{[\rho\to 0]}$	$T_c(\mathrm{K})_{[\mathrm{mid}]}$	$\Delta T_c(\mathrm{K})$	$T^*(\mathrm{K})$	s	Δs
0.13	$\sim$1.2	$\sim$ 2	–	55	–	–
0.135	$\sim$ 1.5	$\sim$ 2	–	–	–	–
0.14	14.0	15.4	2.5	–	2.11	0.15
0.15	19.0	19.5	0.6	42	2.60	0.25
0.16	17.4	18.0	0.9	30	2.45	0.25
0.17	15.4	16.7	1.9	24	2.60	0.25
0.18	12.4	12.9	1.1	15.5	2.33	0.1
0.19	10.8	11.2	0.9	10.5	2.45	0.2

the resistivity data taken in various fixed fields should collapse onto a single curve, from which a value for T_g and $\nu(z-1)$ can be obtained. The modified scaling expression given in Eq. (1) was very successful in accurately describing the data. The data for all the concentrations in this study also scale according to this relation and this is shown in the plots in Fig. (11). Although both scaling models give results that are reasonably consistent with respect to the value of the critical temperature T_g, the temperature range over which the data could be fit to the expression from the RRA scaling model was much clearer than that of the expression from the FFH model. As such, there was much less uncertainty in the values of $\nu(z-1)$ obtained from the RRA model. Values of the exponent $\nu(z-1)$ obtained via the RRA scaling analysis are given in Table I. The significantly better fits to the data from the RRA model leads us to conclude that, for the $Sm_{2-x}Ce_xCuO_{4-y}$ system, the melting of the solid vortex state is significantly influenced by the effects of the magnetic field on the pinning landscape. While it is tempting to attribute this finding to the presence of the Sm sublattice, it is not readily discernible as to whether or not this unusual behavior can be attributed to an interaction of the flux line lattice with the Sm^{3+} ions. However, since the Néel temperature $T_N \sim 6$ K of the Sm sublattice is below that of the majority of the length of the $H_g(T)$ lines, the antiferromagnetic ordering of the Sm^{3+} ions (in the ab-plane) would seem to play no significant role in the dynamical properties of vortices in the region of the melting transition.

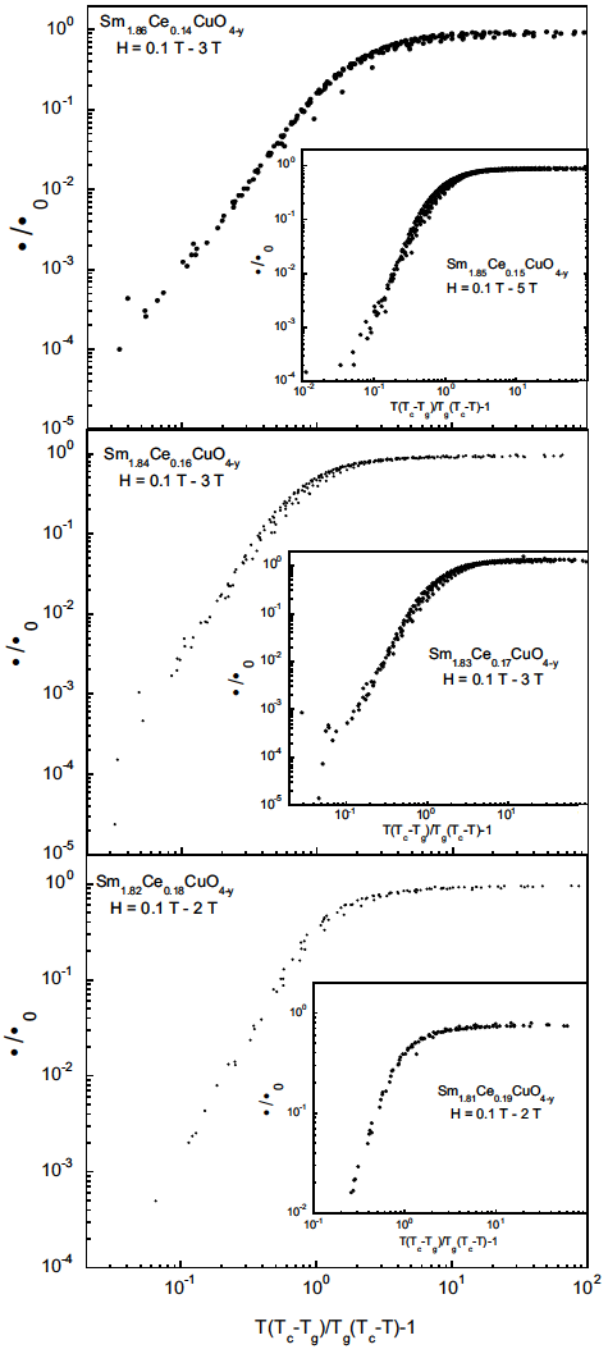

FIG. 11: Resistivity data scaled according to the expression given in Eq. (1) for samples with cerium concentrations between x = 0.14 and x = 0.19.

IV. CONCLUSIONS

Electrical transport measurements were performed on high quality PLD grown epitaxial $Sm_{2-x}Ce_xCuO_{4-y}$ films, from which we have developed further the $H-T-x$ phase diagram of this electron-doped high-T_c superconductor. We find a $T_c - x$ region in good agreement with that found for MBE grown $Sm_{2-x}Ce_xCuO_{4-y}$ films,[2] with the notable difference of higher T_c values obtained in the overdoped region, and subsequently a slight extension of the T_c region to a higher Ce doping level was inferred by us. From an analysis of the in-plane resistivity $\rho_{ab}(T)$ in high magnetic fields we have extended the doping range over which the pseudogap line $T^*(x)$ has been previously determined.[4] The evolution of the boundary

between the solid and liquid vortex phases, $H_g(T)$, was examined for samples with $0.14 \leq x \leq 0.19$ and can be seen to develop towards a form in the overdoped region consistent with the upper critical field $H_{c2}(T)$ of a two-band BCS superconductor.[30] The possible existence of two superconducting bands in $Sm_{2-x}Ce_xCuO_{4-y}$ is further supported by thermopower measurements presented here that are strikingly similar to those obtained on $Pr_{2-x}Ce_xCuO_{4-y}$ films,[12] which, in conjunction with Hall effect measurements, have been cited as evidence supportive of this picture. Finally, from a scaling analysis of the vanishing of the resistivity $\rho(T)$ along the $H_g(T)$ boundary, we find an unusually strong effect of the applied field on the pinning landscape of the vortex flux line lattice.

V. ACKNOWLEDGEMENTS

This research was sponsored by the U.S. Department of Energy (DOE) under Research Grant No. DE-FG02-04ER46105. A portion of this work was performed at the National High Magnetic Field Laboratory, which is supported by NSF Cooperative Agreement No. DMR-0084173, by the State of Florida, and by the DOE.

[1] N. P. Armitage, P. Fournier, and R. L. Greene, cond-mat arXiv:0906.2931 (2009).
[2] Y. Krockenberger, J. Kurian, A. Winkler, A. Tsukada, M. Naito, and L. Alff, Phys. Rev. B **77**, 060505(R) (2008).
[3] T. Kawakami, T. Shibauchi, Y. Terao, M. Suzuki, and L. Krusin-Elbaum, Phys. Rev. Lett. **95**, 017001 (2005).
[4] T. Kawakami, T. Shibauchi, Y. Terao, and M. Suzuki, Phys. Rev. B **74**, 144520 (2006).
[5] S. R. Park, Y. S. Roh, Y. K. Yoon, C. S. Leem, J. H. Kim, B. J. Kim, H. Koh, H. Eisaki, N. P. Armitage, and C. Kim, Phys. Rev. B **75**, 060501(R) (2007).
[6] A. Zimmers, Y. Noat, T. Cren, W. Sacks, D. Roditchev, B. Liang, and R. L. Greene, Phys. Rev. B **76**, 132505 (2007).
[7] M. Ikeda, T. Yoshida, A. Fujimori, M. Kubota, K. Ono, Hena Das, T. Saha-Dasgupta, K. Unozawa, Y. Kaga, T. Sasagawa, and H. Takagi, Phys. Rev. B **80**, 014510 (2009).
[8] M. M. Korshunov, E. V. Zakharova, I. A. Nekrasov, Z. V. Pchelkina, and S. G. Ovchinnikov, J. Phys.: Condens. Matter **22**, 015701 (2010).
[9] I. W. Sumarlin, S. Skanthakumar, J. W. Lynn, J. L. Peng, Z. Y. Li, W. Jiang and R. L. Greene, Phys. Rev. Lett. **68**, 2228 (1992).
[10] S. D. Wilson, P. Dai, S. Li, S. Chi, H. J. Kang, and J. W. Lynn, Nature **442**, 59 (2006).
[11] S. D. Wilson, S. Li, H. Woo, P. Dai, H. A. Mook, C. D. Frost, S. Komiya, and Y. Ando, Phys. Rev. Lett. **96**, 157001 (2006).
[12] P. Li, K. Behnia, and R. L. Greene, Phys. Rev. B **75**, 020506(R) (2007).
[13] E. A. Early, *Ph.D. Thesis* University of California, San Diego (1991).
[14] H. J. Kang, P. Dai, B. J. Campbell, P. J. Chupas, S. Rosenkranz, P. L. Lee, Q. Huang, S. Li, S. Komiya, and Y. Ando, Nature Materials **6**, 224 (2007).
[15] H. S. Yang, Y. S. Chai, J. Liu, M. Yu, P. C. Li, L. Zhang, M. D. Li, and L. Z. Cao, Physica C **403**, 203 (2004).
[16] Y. Dagan, M. M. Qazilbash, C. P. Hill, V. N. Kulkarni, and R. L. Greene, Phys. Rev. Lett. **92**, 167001 (2004).
[17] T. Helm, M. V. Kartsovnik, M. Bartkowiak, N. Bittner, M. Lambacher, A. Erb, J. Wosnitza, and R. Gross, Phys. Rev. Lett. **103**, 157002 (2009).
[18] S. E. Sebastain, N. Harrison, E. Palm, T. P. Murphy, C. H. Mielke, R. Liang, D. A. Bonn, W. N. Hardy, and G. G. Lonzarich, Nature **454**, 200 (2008).
[19] N. Doiron-Leyraud, C. Proust, D. LeBoeuf, J. Levallios, J. -B. Bonnemaison, R. Liang, D. A. Bonn, W. N. Hardy, and L. Taillefer, Nature **447**, 565 (2007).
[20] D. LaBoeuf, N. Doiron-Leyraud, J. Levallois, R. Daou, J. -B. Bonnemaison, N. E. Hussey, L. Balicas, B. J. Ramshaw, R. Liang, D. A. Bonn, W. N. Hardy, S. Adachi, C. Proust, and L. Taillefer, Nature **450**, 533 (2007).
[21] G. S. Boebinger, Y. Ando, A. Passner, T. Kimura, M. Okuya, J. Shimoyama, K. Kishio, K. Tamasaku, N. Ichikawa, and S. Uchida, Phys. Rev. Lett. **77**, 5417 (1996).
[22] P. Fournier, P. Mohanty, E. Maiser, S. Darzens, T. Venkatesan, C. J. Lobb, G. Czjzek, R. A. Webb, and R. L. Greene, Phys. Rev. Lett. **81**, 4720 (1998).
[23] K. Jin, B. Y. Zhu, B. X. Wu, J. Vanacken, V. V. Moshchalkov, B. Xu, L. X. Cao, X. G. Qiu, and B. R. Zhao, Phys. Rev. B **77**, 172503 (2008).
[24] B. X. Wu, K. Jin, J. Yuan, H.B. Wang, T. Hatano, B.R. Zhao, and B.Y. Zhu, Physica C **469**, 1945 (2009).
[25] B. J. Taylor and M. B. Maple, Phys. Rev. B **76**, 014517 (2007).
[26] B. J. Taylor, R. E. Baumbach, D. J. Scanderbeg, and M. B. Maple, Phys. Rev. Lett **xx**, xxxxxx (2010).
[27] T. Timusk and B. Statt, Rep. Prog. Phys. **62**, 61 (1999).
[28] M. R. Norman, D. Pines, and C. Kallin, Adv. Phys. **54**, 715 (2005).
[29] M. B. Maple, C. C. Almasan, C. L. Seaman, S. H. Han, K. Yoshiara, M. Buchgeister, L. M. Paulius, B. W. Lee, D. A. Gajewski, R. F. Jardim, C. R. Fincher, Graciela B. Blanchet, and R. P. Guertin, J. Supercond. **7**, 97 (1994).
[30] M. Mansor and J. P. Carbotte, Phys. Rev. B **72**, 024538 (2005).
[31] D. S. Fisher, M. P. A. Fisher, and D. A. Huse, Phys. Rev. B. **43**, 130 (1991).
[32] A. Rydh, Ö. Rapp, and M. Andersson, Phys. Rev. Lett. **83**, 1850 (1992).
[33] M. Andersson, A. Rydh, and Ö. Rapp, Phys. Rev. B **63**, 184511 (2001).